Journal of Energy Chemistry 50 (2020) 307–313

Contents lists available at ScienceDirect

Journal of Energy Chemistry

journal homepage: www.elsevier.com/locate/jechem

http://www.journals.elsevier.com/journal-of-energy-chemistry/

# Surface charging activated mechanism change: A computational study of O, CO, and $CO_2$ interactions on Ag electrodes

Ilker Tezsevin[a,b], Mauritius C. M. van de Sanden[a,c], Süleyman Er[a,b,*]

[a] DIFFER – Dutch Institute for Fundamental Energy Research, De Zaale 20, Eindhoven 5612 AJ, The Netherlands
[b] CCER – Center for Computational Energy Research, DIFFER – Dutch Institute for Fundamental Energy Research, De Zaale 20, Eindhoven 5612 AJ, The Netherlands
[c] Department of Applied Physics, Eindhoven University of Technology, Eindhoven 5600 MB, The Netherlands

ARTICLE INFO

*Article history:*
Received 17 January 2020
Revised 20 March 2020
Accepted 29 March 2020
Available online 12 April 2020

*Keywords:*
Density functional theory
$CO_2$ reduction
Silver electrode
Surface charge

ABSTRACT

Electrocatalytic and plasma-activated processes receive increasing attention in catalysis. Density functional theory (DFT) calculations are state-of-the-art tools for the fundamental study of reaction mechanisms and predicting the performance of catalytic materials. Proper application of DFT-based methods is crucial when investigating charge-doped electrode surfaces during electrocatalytic and plasma-activated reactions. Here, as a model electrode for plasma-activated $CO_2$ splitting, we studied the interactions of O, CO, and $CO_2$ with the neutral and progressively charged Ag(111) metal surfaces. We show that the application of correction procedures is necessary to obtain accurate adsorption energy profiles of O atoms, CO and $CO_2$ molecules on Ag surfaces that are under the influence of additional electrons. Interestingly, the oxidation of CO is found to shift from a Langmuir–Hinshelwood mechanism on a neutral electrode to an Eley–Rideal mechanism on charged electrodes. Furthermore, we show that the surface charging of Ag(111) electrodes increase their $CO_2$ reduction performance by enhancing the adsorption of O atoms and desorption of CO molecules. A further increase in the absolute charge-state of the electrode surface is expected to waive the thermodynamic barriers for the $CO_2$ splitting reaction.



## 1. Introduction

Rising energy demand, atmospheric pollution, and global warming have drawn intensive attention and increasing investments for more than three decades [1]. The energy demand results in an increase in atmospheric carbon dioxide ($CO_2$) concentrations, which in turn negatively contributes to atmospheric pollution and global warming. To restrain the environmental effects of $CO_2$ meanwhile meeting the future energy needs, new approaches have to be developed to curb the emission, capture, storage, and utilization of $CO_2$ [2–4]. Development of renewable production of carbon-neutral fuels is a way to achieve $CO_2$ emission targets [5–8]. Captured $CO_2$ can be converted into carbon monoxide (CO) that can be utilized as a building block for the synthesis of liquid hydrocarbons via the Fischer–Tropsch process [9–11]. However, the conversion of $CO_2$ to CO or other desirable chemicals requires an energy input and the inert properties of $CO_2$ molecules make this conversion difficult under practical conditions [1,12].

Electrocatalysis draws increasing attention due to its effectiveness in reducing $CO_2$ to CO at atmospheric pressure and room temperature. Since the 1980s, Au and Ag electrodes have been studied as electrocatalysts for $CO_2$ reduction with CO selectivity of up to 100% [1,4,13–15]. Albeit the highly promising selectivity of these electrocatalysts, the efficiencies of conversion reactions were found to suffer from large potentials and slow reaction kinetics, which are due to the low local concentration of $CO_2$ in the proximity of electrocatalysts [15–20]. Thence, $CO_2$ electrocatalysis is not yet fully practical [3,16,17] for industrial use, and to design efficient electrocatalysts new research efforts are needed for a better understanding of the fundamentals of electrocatalytic materials and their surface reactions with atoms and molecules [1,4,21,22].

In addition to the blooming field of electrocatalysis, other new technologies for the conversion of $CO_2$ to CO have been proposed, including the use of non-thermal plasmas for $CO_2$ molecule activation.

$$CO_2 \leftrightarrows CO + \tfrac{1}{2}O_2 \quad (1)$$

* Corresponding author at: DIFFER – Dutch Institute for Fundamental Energy Research, De Zaale 20, Eindhoven 5612 AJ, the Netherlands.
*E-mail address:* s.er@differ.nl (S. Er).

https://doi.org/10.1016/j.jechem.2020.03.080

The use of plasma activation is interesting as it enables the splitting of $CO_2$ into CO, a chemical building block, as shown in Eq. (1) [7,23–28]. Unlike conventional electrocatalytic processes, the plasma process uses gas-phase $CO_2$ feeding without the requirement of the use of water or hydrogen as solvent or co-reactant. However, plasma-assisted $CO_2$ reduction suffers from the recombination of CO and O at the plasma outlet [7,26,29]. The plasma processes can also be coupled with membrane reactors or solid oxide cells (SOC), to benefit from the advantages of different technologies [9,27,29–36]. The combined approaches increase the $CO_2$ conversion either by acting as "atomic oxygen scavengers" that mitigate recombination reactions or by contributing to surface-activated catalytic dissociation of $CO_2$ or both. When these cutting-edge $CO_2$ conversion methods are coupled with renewable electricity generators from solar and wind power, they enable the storage of surplus renewable energy in the chemical bonds of compounds and contribute to the completion of the carbon cycle [32,37–41].

The computational chemistry tools and their applications on materials design for electrochemical transformations have shown significant progress over the past few decades [4]. However, it is still a challenge to perform electronic structure calculations on charged surfaces using well-established planewave basis density functional theory (DFT) codes, principally due to the long-range Coulombic interactions between periodic images of surface slabs. Accordingly, the amount of studies that consider the binding and the reactions of molecules on the charged surfaces are scarce [42]. Howbeit, with the application of correction procedures [42–47] it is possible to use periodic DFT calculations for the study of catalytic surfaces with additional charges.

In literature, Ag is known as both good thermocatalyst for CO oxidation and good electrocatalyst for $CO_2$ to CO reduction [1,15,17,39,48–50]. Accordingly, here we studied the interactions of O, CO, and $CO_2$ with Ag metal electrodes under the influence of additional electrons. As the coupling of CO with O is a known issue of the plasma splitting of $CO_2$, a study on catalytic behavior of the charged Ag electrodes should cover both the forward and backward directions shown in Eq. (1). Since this reaction does not involve the use of a solvent or co-reactant, the presence of chemical species, such as $H_2$ or $H_2O$, has not been considered in the current study.

## 2. Computational methods

We used Vienna *ab-initio* Simulation Package (VASP) to perform all DFT calculations reported in the current work [51–53]. The projector augmented wave (PAW) method was employed to describe electron-ion interactions. A kinetic energy cutoff of 500 eV was used for the planewave basis for all calculations [54,55]. We used the Perdew-Burke-Ernzerhof (PBE) exchange-correlation functional of the generalized gradient approximation (GGA) [56]. The convergence criteria for structural optimizations were that the total forces acting on each atom must be smaller than 0.015 eV/Å. The Brillouin zone of crystalline Ag metal is integrated using an automatically generated 33 × 33 × 33 Monkhorst–Pack *k*-point mesh [57]. The optimized lattice parameter of Ag with Fm-3 m space group is 4.15 Å, which is in good agreement with the experimental value of 4.09 Å [58]. The (111) surface is the thermodynamically most stable and therefore the most common surface structure of *fcc* metals [59]. A fully periodic Ag(111) surface slab was generated by using a 3 × 3 supercell with five atomic layers, therefore totaling to 45 Ag atoms per supercell. Ag atoms at the bottom two layers were kept fixed in their optimized bulk lattice positions, whereas the atoms in the top three slab layers were allowed to relax. Periodicity of the slab in the direction perpendicular to the metal surface was avoided by adding a vacuum spacing of 15 Å. Different ($N \times N \times 1$) k-point meshes have been tested for their influence on the convergence of total energy of Ag(111) slabs, and the 4 × 4 × 1 *k*-point mesh is found to be a reasonable choice when considering both computational cost and accuracy, for which the deviation from denser *k*-point sets was less than 0.002 eV per Ag atom. The zero damping DFT–D3 method of Grimme was used to include the van der Waals interactions between the Ag(111) surface and molecules [60].

The adsorption energies of the adsorbates on Ag(111) surfaces have been calculated using

$$E_{\mathrm{Ads}} = E_{\mathrm{slab+adsorbate}} - (E_{\mathrm{slab}} + E_{\mathrm{adsorbate}}) \quad (2)$$

where $E_{\mathrm{slab+adsorbate}}$ is the total energy of Ag(111) slab with adsorbate at its lowest energy position on the metal surface, $E_{\mathrm{slab}}$ is the total energy of clean Ag(111) slab, and $E_{\mathrm{adsorbate}}$ is the total energy of CO or $CO_2$ molecules or half of the total energy of $O_2$ molecule. Energies of the adsorbate molecules were computed via spin relaxed calculations in 15 Å cubic cells. The structures of the optimized reactants and products on the metal surfaces are used as inputs for the climbing image nudged elastic band (CI-NEB) [61] calculations aimed at the study of transition states and calculation of energy barriers between CO and $CO_2$ conversions.

## 3. Results and discussion

The (111) surface is the thermodynamically most stable surface for *fcc* metals, including Ag [59]. On Ag(111) surface, there are four different adsorption sites, i.e. *metal top, bridge, fcc hollow* and *hcp hollow* (see Fig. S1) [59,62]. We studied the adsorption of O, CO, and $CO_2$ molecules on the four different adsorption sites and by considering various adsorbate orientations. We found that the lowest energy adsorption sites for O and CO are *fcc hollow* and *metal top* sites, respectively, both in perfect agreement with earlier studies [63,64]. Additionally, we found that the adsorption of $CO_2$ on Ag(111) surface is energetically not favorable, which is also in accordance with experiments [65,66].

Counting the number of excess electrons on metal electrodes is possible in experiments. For instance, for Pt metal nanoparticles on a support, a net charge transfer of $1.2 \times 10^{14}$ $e^-/cm^2$ has been reported [67]. Comparing to a cathode that operates at a typical SOC current density [32] of 1 A/cm$^2$, for the Ag(111) surface area as used in our calculations the electron flow will be 41,875 $e^-$/s. Assuming a time constant of 1 ms [68], approximately 42 additional electrons can be accommodated on our model Ag electrodes. Under the plasma effect, the electronic charge on electrodes is expected to increase further [38]. For our model system, which is a 3 × 3 Ag(111) surface with nine Ag atoms, an additional electron corresponds to an electron density of $1.49 \times 10^{15}$ $e^-/cm^2$. In our DFT calculations, we added an increasing number of two, four, and six additional electrons to the 45 metal atom slabs, which result in electron densities of approximately $2.98 \times 10^{15}$, $5.96 \times 10^{15}$ and $8.94 \times 10^{15}$ $e^-/cm^2$, respectively. In addition to the electron-doped surfaces, we also considered the clean Ag surface with no added electrons for the study of molecule interactions. As shown in Fig. S2, without the added electrons, the charge distribution amongst the metal layers show a largely symmetric distribution between the top and bottom layers. When additional electrons are introduced, the localization of charge on the two faces of the slab follow a similar trend as for the neutral surface (see Fig. S2). In other words, the added electrons are not only hosted on the top layer but also on the bottom layer and to a lesser amount on the mid-layers of the electrode. On neutral surfaces, the periodic DFT calculated adsorption energies of molecules, such as CO, are independent of the sufficiently large vacuum lengths ($L$). However, for charged surfaces, as shown in Fig. S3, due to Coulomb interactions, the adsorption energies of CO are linearly proportional to the inverse of vacuum spacing between slabs ($1/L$) [42].

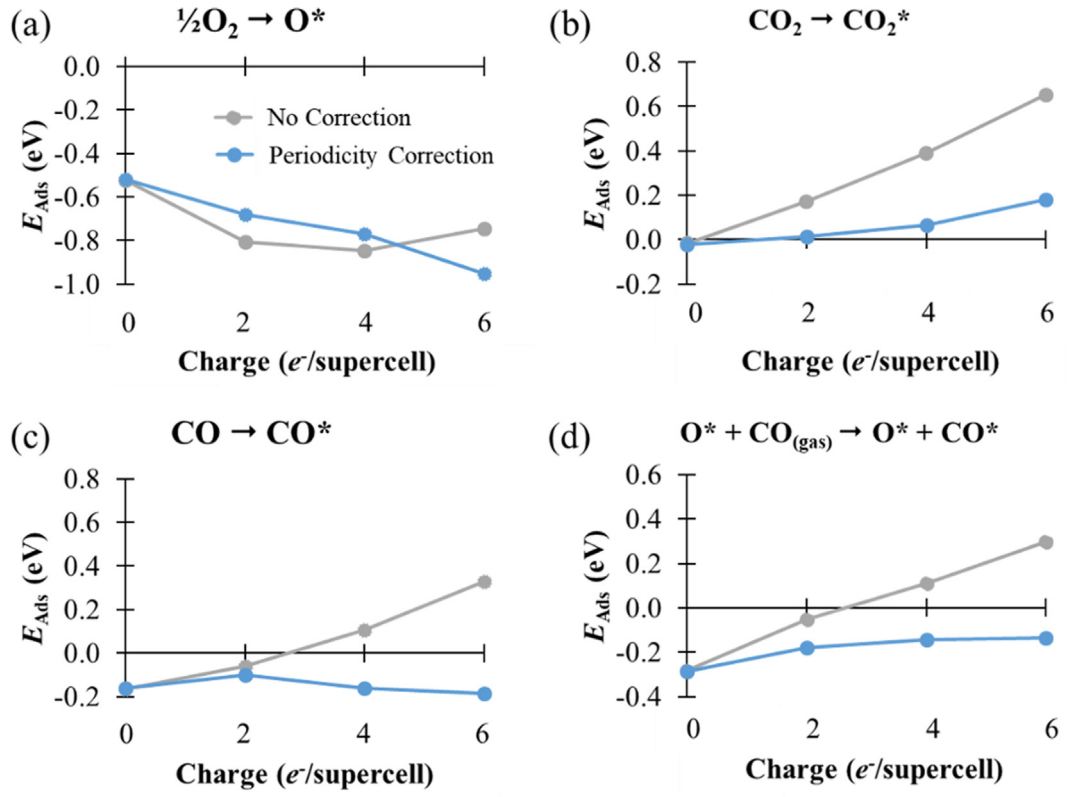


**Fig. 1.** Adsorption energies of (a) O, (b) $CO_2$, and (c) CO on clean surface, and (d) CO on O-adsorbed surface (see Table S1 for numerical data).

The common periodic DFT codes can usually be configured to add a homogeneous background charge when the total number of electrons used in calculations are different than that of a neutral slab [69]. This, however, by itself is not sufficient for the accurate calculation of adsorption energies of chemical species on the charged surfaces of electrodes. To surmount errors associated with Coulomb interactions between periodically repeating images in the perpendicular direction to catalyst surface, for CO molecules on Ag(111), we initially used vacuum spacings of 15, 20, 30, 40, 50, and 60 Å and extrapolated the adsorption energies to the infinite vacuum ($L\rightarrow\infty$). As shown in Fig. S4, using only two different vacuum spacings of 15 and 30 Å were sufficient in predicting the corrected adsorption energies that have been calculated using additional vacuum spacings. Therefore, we performed the calculations aimed at the study of adsorption of all other chemical species, with 15 and 30 Å vacuum spacings. To obtain the corrected adsorption energies at the infinite vacuum, the DFT calculated results are incorporated into the following equation

$$E_{Ads}^{PC} = E_{Ads}^{II} - \frac{1}{L_{II}}\left(\frac{E_{Ads}^{II} - E_{Ads}^{I}}{1/L_{II} - 1/L_{I}}\right) \quad (3)$$

where $E_{Ads}^{PC}$ is the periodicity-corrected adsorption energy at the infinite vacuum, $E_{Ads}^{I}$ and $E_{Ads}^{II}$ are the adsorption energies calculated with two different vacuum lengths, $L_I$ and $L_{II}$.

We found that the application of periodicity corrections on the charged Ag surface has a significant impact on the computed results. As shown in Fig. 1(a), when the additional charge on the metal slab is raised, the O adsorption becomes increasingly stronger and at four $e^-$/supercell additional charge the $E_{Ads}(O)$ reaches its minima, and increases for six $e^-$/supercell. The $E_{Ads}(CO_2)$ on the neutral surface is slightly below zero (–0.02 eV), as shown in Fig. 1(b), and increases with an increase of additional surface charge. CO binds to both clean and oxygenated Ag(111) surfaces favorably. As shown in Fig. 1(c, d), an increase in the number of added $e^-$ results in a less favorable CO adsorption. Interestingly, on both clean and oxygen adsorbed surfaces, with the addition of four and six $e^-$/supercell, the CO adsorption becomes energetically not favorable. Next, we performed the second set of calculations with 30 Å vacuum length between metal slabs and incorporated their results together with the results of 15 Å vacuum calculations into Eq. (3). Compared to the results without correction, when the periodicity correction is applied, the O adsorption energy on two and four $e^-$/supercell doped-surfaces increases, while on six $e^-$/supercell doped-surface it decreases. After applying the periodicity correction, the O adsorption energy versus surface charge shows a different profile, as shown with blue circles in Fig. 1(a). $CO_2$ adsorption, on the other hand, follows an almost linear adsorption energy trend in the energetically unfavorable region after applying the periodicity correction. However, the periodicity-corrected results produce lower $CO_2$ adsorption energies and are less sensitive to additional surface charge. The CO adsorption profile shows an interestingly different behavior after the periodicity corrections. CO adsorption energies reach their maxima with two $e^-$/supercell and they decrease as surface charge increases. As shown in Fig. 1(d), the periodicity corrections for CO adsorption on the oxygenated surfaces have a similar effect to that of $CO_2$ adsorption. Unlike the results as predicted by routine DFT calculations, the CO adsorption on the oxygenated surfaces is energetically favorable for all the charged systems that are covered in the present study. According to these findings, as the surface charge increases, the disparities between the routine and corrected calculation results become more serious. Therefore, correction procedures for periodic DFT calculations are essentially needed for the study of charged electrodes and their interactions with molecules.

To study the effects of surface charging of Ag electrodes on the reaction energetics, we considered Eq. (1) for both the CO and

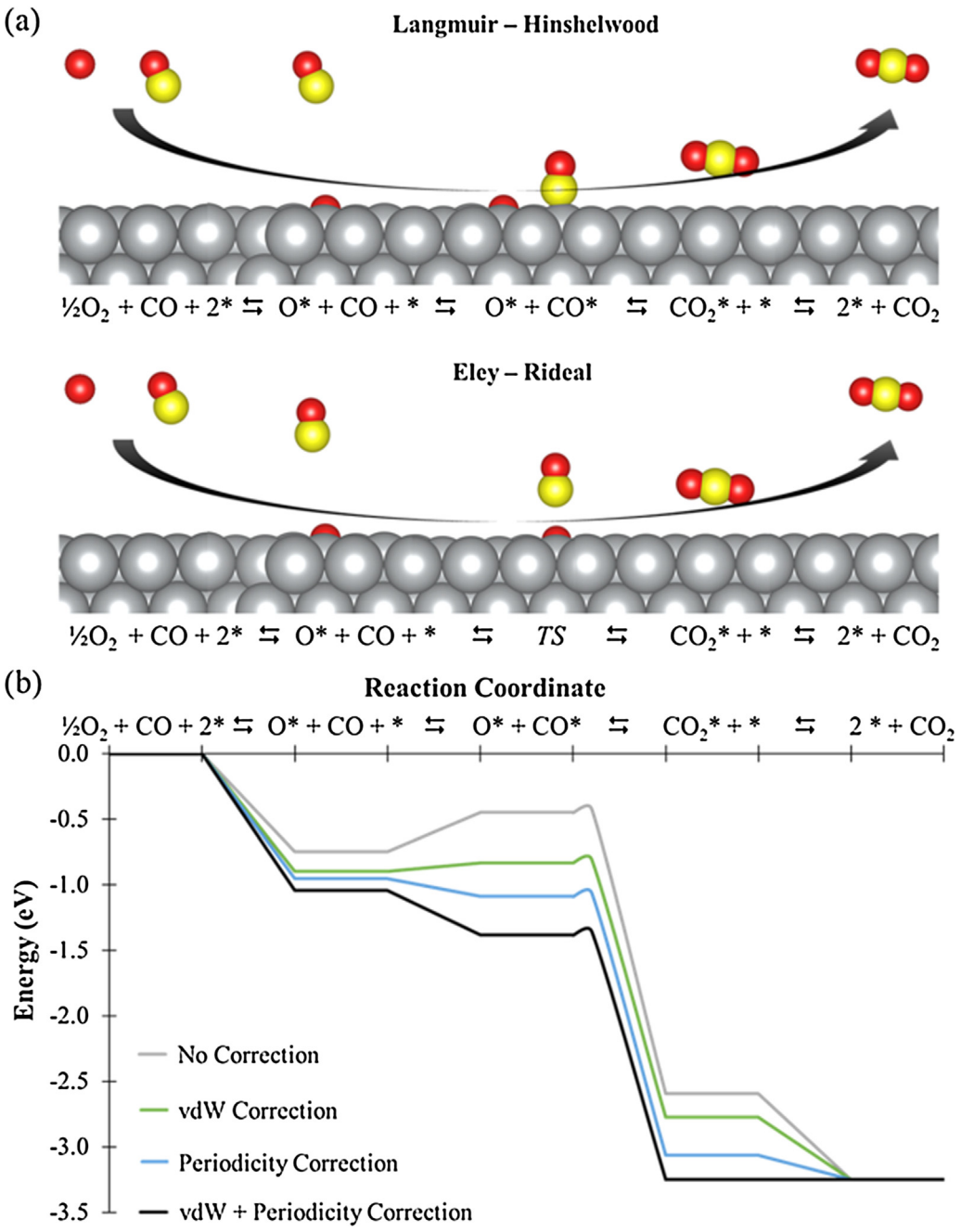


**Fig. 2.** (a) LH and ER reaction mechanisms for CO oxidation on Ag(111) surface (TS represents transition state for the ER mechanism), (b) effect of calculation procedure on the energy profile of CO + ½$O_2$ ⇆ $CO_2$ on six $e^-$/supercell (corresponding to 8.94 × $10^{15}$ $e^-/cm^2$) charged Ag electrode. Energies are relative to the Ag(111) slab with six $e^-$/supercell additional charge and a neutral $CO_2$ molecule in the gas-phase.

O recombination (CO oxidation) and the $CO_2$ dissociation ($CO_2$ reduction) pathways. For the oxidation reaction, when CO and O co-exist in the reaction medium since the absolute of O adsorption energy (–0.52 eV) is significantly larger than CO adsorption energy (–0.16 eV) on the electrode surface, the purely thermodynamic results dictate that O atoms would be adsorbed on Ag surface before CO molecules. To produce $CO_2$, the CO molecules then need to interact with the adsorbed O (i.e. O*) atoms via either Langmuir–Hinshelwood (LH) or Eley–Rideal (ER) mechanisms, as shown in Fig. 2(a). The favorable oxidation mechanism on the surface is determined by the competition between the activation energy of the direct interaction of $CO_{(gas)}$ with O* and the adsorption energy of CO to oxygenated surface. We found that the CO and O co-adsorption step does not involve an activation barrier. A negative CO adsorption energy dictates that the reaction should proceed via LH mechanism. When CO adsorption to the oxygenated surface is positive and larger than the activation barrier for $CO_{(gas)}$ + O* reaction, then the reaction follows ER mechanism. The importance of the application of correction schemes to periodic DFT calculations of charged electrodes becomes more obvious at this step. As reported in Table S1, we also performed calculations by taking into account the van der Waals (vdW) interactions. To signify the necessity of periodicity corrections, we have not included vdW interactions in Fig. 1. To achieve accurate reaction mechanism energetics, we include the vdW contributions as well in the comparisons below. In Fig. 2(b), a comparison of the full reaction path-

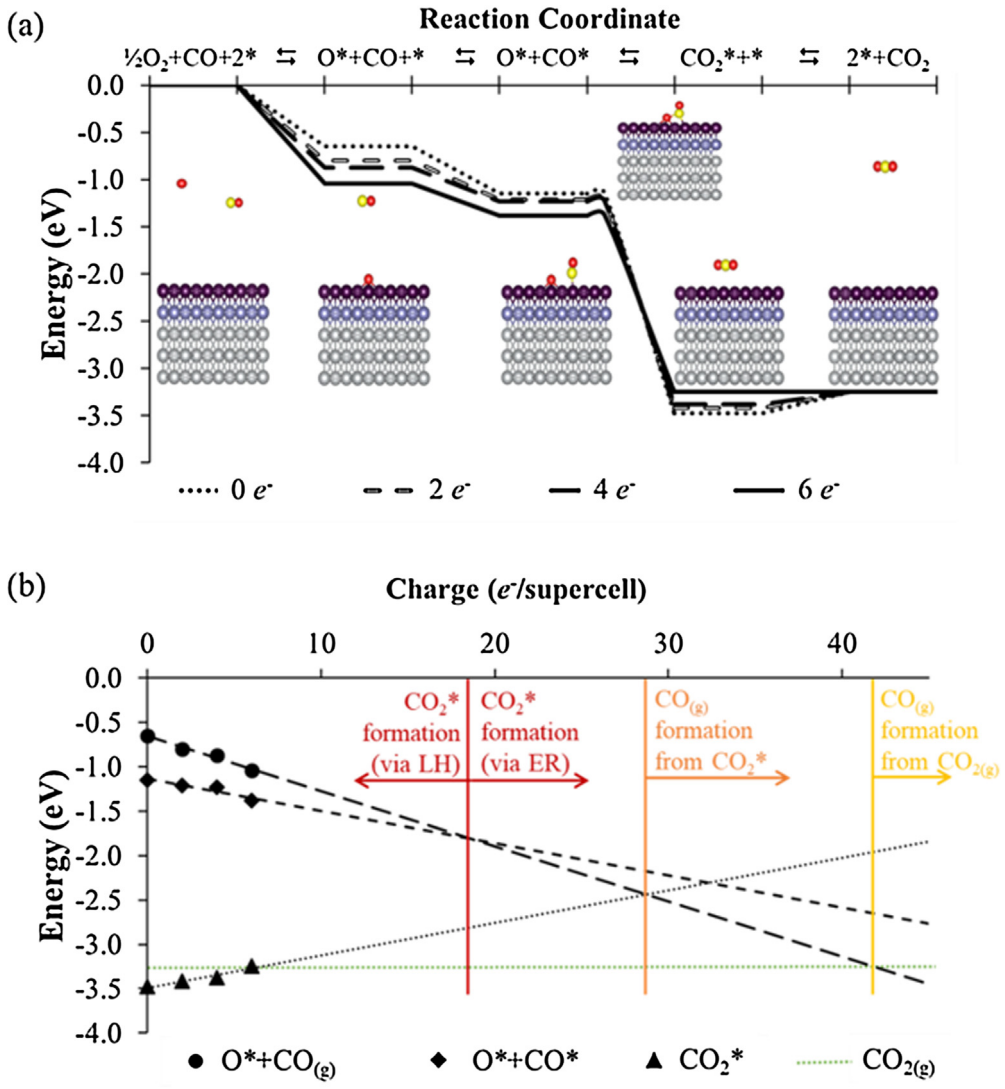


**Fig. 3.** (a) Effect of surface charging on O, CO, and $CO_2$ interactions with Ag(111) surfaces with zero, two, four, and six added electrons per supercell. (b) Projection of surface charging effect on relative energies of the species during reaction. Energies are relative to the sum of respective charged state of Ag(111) slab energy, neutral CO and $½O_2$ molecule energies in the gas-phase. Green dotted line shows the relative energy of the sum of respective charged state of Ag(111) slab energies and gas-phase $CO_2$ molecule.

way energetics, under the influence of six $e^-$/supercell additional charge, as calculated by four different computational procedures is presented. According to DFT calculations with no corrections and calculations with vdW contributions, the CO and O co-adsorption is less favorable when compared to $CO_{(gas)}$ and O*. Hence, the oxidation reaction should follow the ER mechanism. However, when periodicity corrections or periodicity corrections with vdW contributions are included, the co-adsorption becomes more favorable and the oxidation reaction follows the LH mechanism. These results show that periodic DFT calculations on charged systems without proper correction procedures might lead to deceptive mechanistic results as well as the energetics as discussed above.

Fig. 3(a) shows the formation of $CO_2$ on charged Ag(111) electrodes that have been calculated using both vdW contributions and periodicity corrections. On the clean slab, the calculated activation barrier for the oxidation reaction between CO* and O* to produce $CO_2$* is 0.14 eV. Injection of additional electrons to the Ag electrode decreases the activation barrier to 0.04 eV, thus making the oxidation step more favorable than on neutral electrodes. For the reduction reaction shown in Eq. (1), the activation barrier between $CO_2$*, and co-adsorbed CO* and O* are calculated as 2.33, 2.22, 2.16, and 1.87 eV, respectively for supercells with zero, two, four, and six additional electrons. As the surface charging increases, the CO* desorption energies decrease from 0.50 consecutively to 0.40, 0.36 and 0.34 eV. Accordingly, the addition of electrons to the Ag slab decreases the barriers for the formation and desorption of CO molecules (Fig. 3a). For the additional charge range that has been covered in the current study, the reaction shown in Eq. (1) proceeds in the oxidation direction via the LH mechanism (Fig. 3b). Nevertheless, during plasma- and electro-catalytic chemical conversion experiments, the electrodes might well experience additional charges on their surfaces that are beyond the number of added electrons that have been considered in the current study [38]. However, due to practical limitations (see Fig. S2), we have not considered further charging of the surface beyond six $e^-$/supercell. To estimate the effect of higher charge contributions on $CO_2$ reduction, inspired by the linear profile of our results as shown in Fig. 3(b), we extrapolated the relative energies of O adsorption, CO and O co-adsorption, and $CO_2$ adsorption, as calculated with respect to the energy of the clean Ag-surface at a given charge state plus neutral CO and $½O_2$ molecule energies in the gas-phase. According to these projected results shown

in Fig. 3(b), the LH oxidation reaction is the energetically favorable mechanism up to 19 $e^-$/supercell. When the additional charge reaches 19 $e^-$/supercell, the $E_{Ads}$ for O becomes equivalent to that of O and CO co-adsorption. For farther charging than this point, the CO adsorption to the oxygenated surface is expected to become an activation barrier itself for the LH oxidation reaction, and therefore the reaction mechanism is expected to shift to an ER reaction. When the additional charge exceeds 29 $e^-$/supercell, the adsorption of molecular $CO_2$ on the Ag surface becomes energetically unfavorable when compared to its dissociation into $O^*$ and $CO_{(gas)}$ molecule. Finally, assuming that a linear profile would still be valid, the charging of the Ag electrode to beyond 42 $e^-$/supercell will ease the reduction of gas-phase $CO_2$ into $O^*$ and $CO_{(gas)}$.

## 4. Conclusions

In summary, we studied the interactions of O, CO and $CO_2$ with the neutral and electrically charged Ag(111) surfaces and showed the importance of proper correction procedures for the calculation of adsorption energies and reaction mechanisms, and ultimately the computer-aided prediction of catalytic behavior of charged catalysts. We found that when CO, O and $CO_2$ mixtures interact with Ag(111) surfaces, both the direction of the reaction and the nature of the reaction mechanism can be modulated by the tuning the concentration of surface electrons. For the CO oxidation reaction, for both neutral and charged Ag(111) electrodes up until approximately 19 $e^-$/supercell additional charge, the LH mechanism is favored, whereas between 19 and 29 $e^-$/supercell the ER mechanism is energetically favored. At higher surface electron concentrations, such as when the additional charge is larger than 29 $e^-$/supercell, the reduction of $CO_2$ molecules would become energetically favorable than their adsorption on the electrode surface. Finally, when additional charge exceeds 42 $e^-$/supercell, the production of $CO_{(g)}$ would become thermodynamically favorable. Unique for the $CO_2$ conversion on charged Ag electrodes as investigated here, by applying a proper correction scheme, we showed that the transition from an oxidation catalyst to a reduction catalyst require substantially higher charging of the metal surface with electrons than the case when no correction scheme is used. The methodology employed here is in principle applicable to the computational study of any conversion reaction on charged electrodes of various kinds.

## Declaration of Competing Interest

The authors declare that they have no known competing financial interests or personal relationships that could have appeared to influence the work reported in this paper.

## Acknowledgments

The work presented in this paper is part of the European project KEROGREEN, which has received funding from the European Union's Horizon 2020 Research and Innovation Programme under Grant Agreement no. 763909. SE acknowledges funding from the initiative "Computational Sciences for Energy Researcah" of Shell and the Netherlands Organization for Scientific Research (NWO) grant no. 15CSTT05. This work was carried out on the Dutch national e-infrastructure with the support of SURF Cooperative.

## Supplementary material

Supplementary material associated with this article can be found, in the online version, at doi:10.1016/j.jechem.2020.03.080.

## References

[1] W. Zhang, Y. Hu, L. Ma, G. Zhu, Y. Wang, X. Xue, R. Chen, S. Yang, Z. Jin, Adv. Sci. 5 (2018) 1700275.
[2] A.P.H. Goede, W.A. Bongers, M.F. Graswinckel, R.M.C.M. Van De Sanden, M. Leins, J. Kopecki, A. Schulz, M. Walker, EPJ Web Conf. 79 (2014) 1–5.
[3] J.T. Feaster, C. Shi, E.R. Cave, T. Hatsukade, D.N. Abram, K.P. Kuhl, C. Hahn, J.K. Nørskov, T.F. Jaramillo, ACS Catal. 7 (2017) 4822–4827.
[4] Z.W. Seh, J. Kibsgaard, C.F. Dickens, I. Chorkendorff, J.K. Nørskov, T.F. Jaramillo, Science 355 (2017) eaad4998 (80-.).
[5] R.J. Detz, J.N.H. Reek, B.C.C. Van Der Zwaan, Energy Environ. Sci. 11 (2018) 1653–1669.
[6] K. Li, B. Peng, T. Peng, ACS Catal. 6 (2016) 7485–7527.
[7] R. Snoeckx, A. Bogaerts, Chem. Soc. Rev. 46 (2017) 5805–5863.
[8] H. Xie, J. Wang, K. Ithisuphalap, G. Wu, Q. Li, J. Energy Chem. 26 (2017) 1039–1049.
[9] A. Lebouvier, S.A. Iwarere, P. D'Argenlieu, D. Ramjugernath, L. Fulcheri, Energy Fuels 27 (2013) 2712–2722.
[10] B. Mondal, P. Sen, A. Rana, D. Saha, P. Das, A. Dey, ACS Catal. 9 (2019) 3895–3899.
[11] O.S. Bushuyev, P. De Luna, C.T. Dinh, L. Tao, G. Saur, J. van de Lagemaat, S.O. Kelley, E.H. Sargent, Joule 2 (2018) 825–832.
[12] Y. Li, S.H. Chan, Q. Sun, Nanoscale 7 (2015) 8663–8683.
[13] Y. Peng, W. Si, J. Li, J. Crittenden, J. Hao, Catal. Sci. Technol. 5 (2015) 2478–2485.
[14] M.R. Singh, J.D. Goodpaster, A.Z. Weber, M. Head-gordon, A.T. Bell, Proc. Nat. Acad. Sci. 114 (2017) E8812–E8821.
[15] Q. Lu, J. Rosen, Y. Zhou, G.S. Hutchings, Y.C. Kimmel, J.G. Chen, F. Jiao, Nat. Commun. 5 (2014) 1–6.
[16] M. Liu, Y. Pang, B. Zhang, P. De Luna, O. Voznyy, J. Xu, X. Zheng, C.T. Dinh, F. Fan, C. Cao, F.P.G. De Arquer, T.S. Safaei, A. Mepham, A. Klinkova, E. Kumacheva, T. Filleter, D. Sinton, S.O. Kelley, E.H. Sargent, Nature 537 (2016) 382–386.
[17] F. Zhou, S. Liu, B. Yang, P. Wang, A.S. Alshammari, Y. Deng, Electrochem. Commun. 46 (2014) 103–106.
[18] C. Kim, T. Eom, M.S. Jee, H. Jung, H. Kim, B.K. Min, Y.J. Hwang, ACS Catal. 7 (2017) 779–785.
[19] Y. Zhou, F. Che, M. Liu, C. Zou, Z. Liang, P. De Luna, H. Yuan, J. Li, Z. Wang, H. Xie, H. Li, P. Chen, E. Bladt, R. Quintero-Bermudez, T.K. Sham, S. Bals, J. Hofkens, D. Sinton, G. Chen, E.H. Sargent, Nat. Chem. 10 (2018) 974–980.
[20] W. Weng, L. Tang, W. Xiao, J. Energy Chem. 28 (2019) 128–143.
[21] N. Todoroki, H. Tei, H. Tsurumaki, T. Miyakawa, T. Inoue, T. Wadayama, ACS Catal. 9 (2019) 1383–1388.
[22] M.B. Ross, P. De Luna, Y. Li, C.-T.T. Dinh, D. Kim, P. Yang, E.H. Sargent, Nat. Catal. 2 (2019) 648–658.
[23] G.J. van Rooij, H.N. Akse, W.A. Bongers, M.C.M. van de Sanden, Plasma Phys. Control. Fusion 60 (2018) 014019.
[24] R. Aerts, W. Somers, A. Bogaerts, ChemSusChem 8 (2015) 702–716.
[25] M.S. Moss, K. Yanallah, R.W.K. Allen, F. Pontiga, Plasma Sources Sci. Technol. 26 (2017) 035009.
[26] A. Berthelot, A. Bogaerts, J. Phys. Chem. C 121 (2017) 8236–8251.
[27] G. Chen, L. Wang, T. Godfroid, R. Snyders, Plasma Chemistry and Gas Conversion, IntechOpen, 2018.
[28] Y. Yin, T. Yang, Z. Li, P. Liu, X. Liu, E.J. Devid, Q. Huang, D. Auerbach, A.W. Kleyn, Plasma Driven Boudouard Reaction for Efficient Chemical Storage, SSRN Electron. J. (2019), doi:10.2139/ssrn.3383798.
[29] D. Zhang, Q. Huang, E.J. Devid, E. Schuler, N.R. Shiju, G. Rothenberg, G. van Rooij, R. Yang, K. Liu, A.W. Kleyn, J. Phys. Chem. C 122 (2018) 19338–19347.
[30] X. Zhu, J.-H. Liu, X.-S. Li, J.-L. Liu, X. Qu, A.-M. Zhu, J. Energy Chem. 26 (2017) 488–493.
[31] X. Tu, J.C. Whitehead, Appl. Catal. B Environ. 125 (2012) 439–448.
[32] A.P.H. Goede, EPJ Web Conf. 189 (2018) 00010.
[33] M. Tou, R. Michalsky, A. Steinfeld, Joule 1 (2017) 146–154.
[34] J. Perez-Carbajo, I. Matito-Martos, S.R.G. Balestra, M.N. Tsampas, M.C.M. van de Sanden, J.A. Delgado, V.I. Águeda, P.J. Merkling, S. Calero, ACS Appl. Mater. Interfaces 10 (2018) 20512–20520.
[35] A. Bogaerts, E.C. Neyts, ACS Energy Lett. 3 (2018) 1013–1027.
[36] Y. Qiu, L. Ma, D. Zeng, M. Li, D. Cui, Y. Lv, S. Zhang, R. Xiao, J. Energy Chem. 46 (2020) 123–132.
[37] M.R. Singh, J.D. Goodpaster, A.Z. Weber, M. Head-Gordon, A.T. Bell, Proc. Natl. Acad. Sci. 114 (42) (2017) E8812–E8821.
[38] A.P.H. Goede, W.A. Bongers, M.F. Graswinckel, R.M.C. van de Sanden, M. Leins, J. Kopecki, A. Schulz, M. Walker, EPJ Web Conf. 79 (2014) 01005.
[39] T. Hatsukade, K.P. Kuhl, E.R. Cave, D.N. Abram, T.F. Jaramillo, Phys. Chem. Chem. Phys. 16 (2014) 13814–13819.
[40] J.T. Feaster, C. Shi, E.R. Cave, T. Hatsukade, D.N. Abram, K.P. Kuhl, C. Hahn, J.K. Nørskov, T.F. Jaramillo, ACS Catal. 7 (2017) 4822–4827.
[41] Y.Y. Birdja, E. Pérez-Gallent, M.C. Figueiredo, A.J. Göttle, F. Calle-Vallejo, M.T.M. Koper, Nat. Energy 4 (2019) 732–745.
[42] K.M. Bal, E.C. Neyts, Phys. Chem. Chem. Phys. 20 (2018) 8456–8459.
[43] F. Che, J.T. Gray, S. Ha, N. Kruse, S.L. Scott, J.-S. McEwen, ACS Catal. 8 (2018) 5153–5174.
[44] S.E. Taylor, F. Bruneval, Phys. Rev. B 84 (2011) 075155.
[45] T.R. Durrant, S.T. Murphy, M.B. Watkins, A.L. Shluger, J. Chem. Phys. 149 (2018) 024103.

[46] C.A. Rozzi, D. Varsano, A. Marini, E.K.U. Gross, A. Rubio, Phys. Rev. B 73 (2006) 205119.
[47] K.M. Bal, S. Huygh, A. Bogaerts, E.C. Neyts, Plasma Sources Sci. Technol. 27 (2018) 024001.
[48] R. Daiyan, X. Lu, Y.H. Ng, R. Amal, ChemistrySelect 2 (2017) 879–884.
[49] H.Y. Su, Z. Zeng, X.H. Bao, W.X. Li, J. Phys. Chem. C 113 (2009) 8266–8272.
[50] X. Lei, G. Mbamalu, C. Qin, J. Phys. Chem. C 121 (2017) 2635–2642.
[51] G. Kresse, J. Furthmüller, Comput. Mater. Sci. 6 (1996) 15–50.
[52] G. Kresse, J. Furthmüller, Phys. Rev. B 54 (1996) 11169–11186.
[53] G. Kresse, J. Hafner, Phys. Rev. B 48 (1993) 13115–13118.
[54] P.E. Blöchl, Phys. Rev. B 50 (1994) 17953–17979.
[55] G. Kresse, D. Joubert, Phys. Rev. B 59 (1999) 1758–1775.
[56] J.P. Perdew, K. Burke, M. Ernzerhof, Phys. Rev. Lett. 77 (1996) 3865–3868.
[57] H.J. Monkhorst, J.D. Pack, Phys. Rev. B 13 (1976) 5188–5192.
[58] L. Liu, W.A. Bassett, J. Appl. Phys. 44 (1973) 1475–1479.
[59] W. Dononelli, T. Klüner, Faraday Discuss. 208 (2018) 105–121.
[60] S. Grimme, J. Antony, S. Ehrlich, H. Krieg, J. Chem. Phys. 132 (2010) 154104.
[61] G. Henkelman, B.P. Uberuaga, H. Jónsson, J. Chem. Phys. 113 (2000) 9901–9904.
[62] Y. He, X.Y. Wei, C.T. Chan, J.G. Che, Phys. Rev. B - Condens. Matter Mater. Phys. 71 (2005) 1–4.
[63] M. Gajdoš, A. Eichler, J. Hafner, J. Phys. Condens. Matter 16 (2004) 1141–1164.
[64] Y. Zhu, X.Y. Zhang, S.H. Zhang, J.K. Yang, C. Han, A.M. Hao, R.P. Liu, Solid State Sci. 14 (2012) 1480–1485.
[65] F. Solymosi, J. Mol. Catal. 65 (1991) 337–358.
[66] S. Wang, X. Liao, D. Cao, C. Huo, Y. Li, J. Wang, H. Jiao, J. Phys. Chem. C 111 (2007) 16934–16940.
[67] Y. Lykhach, S.M. Kozlov, T. Skála, A. Tovt, V. Stetsovych, N. Tsud, F. Dvořák, V. Johánek, A. Neitzel, J. Mysliveček, S. Fabris, V. Matolín, K.M. Neyman, J. Libuda, Nat. Mater. 15 (2016) 284–288.
[68] T.D. Jarvi, E.M. Stuve, Wiley-VCH, Inc., 1998, pp. 75–154.